Published in final edited form as:
Mech Ageing Dev. 2012 September ; 133(9-10): 620–628. doi:10.1016/j.mad.2012.08.002.

Impaired Adaptability of in Vivo Mitochondrial Energetics to Acute Oxidative Insult in Aged Skeletal Muscle

Michael P. Siegel[a], **Tim Wilbur**[b], **Mark Mathis**[b], **Eric Shankland**[b], **Atlas Trieu**[b], **Mary-Ellen Harper**[c], and **David J. Marcinek**[a,b,*]

[a] Department of Bioengineering University of Washington 3720 15th Ave NE Seattle, WA 98195

[b] Department of Radiology University of Washington 1959 NE Pacific St Seattle, WA 98195

[c] Departments of Biochemistry, Microbiology and Immunology, Faculty of Medicine University of Ottawa 451 Smyth Rd Ottawa, ON K1H8M5

Abstract

Periods of elevated reactive oxygen species (ROS) production are a normal part of mitochondrial physiology. However, little is known about age-related changes in the mitochondrial response to elevated ROS in vivo. Significantly, ROS-induced uncoupling of oxidative phosphorylation has received attention as a negative feedback mechanism to reduce mitochondrial superoxide production. Here we use a novel in vivo spectroscopy system to test the hypothesis that ROS-induced uncoupling is diminished in aged mitochondria. This system simultaneously acquires ^{31}P magnetic resonance and near-infrared optical spectra to non-invasively measure phosphometabolite and O_2 concentrations in mouse skeletal muscle. Using low dose paraquat to elevate intracellular ROS we assess in vivo mitochondrial function in young, middle aged, and old mice. Oxidative phosphorylation was uncoupled to the same degree in response to ROS at each age, but this uncoupling was associated with loss of phosphorylation capacity and total ATP in old mice only. Using mice lacking UCP3 we demonstrate that this in vivo uncoupling is independent of this putative uncoupler of skeletal muscle mitochondria. These data indicate that ROS-induced uncoupling persists throughout life, but that oxidative stress leads to mitochondrial deficits and loss of ATP in aged organisms that may contribute to impaired function and degeneration.

Keywords

Mitochondria; Uncoupling; Oxidative Stress; Skeletal Muscle; UCP3

1. Introduction

Mitochondrial dysfunction is implicated in many age-related disorders, including loss of muscle mass and function (sarcopenia) (Marzetti and Leeuwenburgh 2006), exercise intolerance (Conley et al. 2000), and neurodegeneration (Gibson et al. 2010). In humans,

[*]**Corresponding Author:** David J. Marcinek Departments of Radiology and Bioengineering, Box 358050 University of Washington Medical School Seattle, WA 98103, USA dmarc@uw.edu, Tel: 206-221-6785, Fax: 206-616-9878. msiegel1@uw.edutwilbur@uw.edumathis@uw.edushanklan@uw.edumharper@uottawa.ca.

these effects are associated with diminished mobility, reduced quality of life, and stress on health care systems in countries with aging populations (Lang et al. 2010).

The accumulation of oxidative damage resulting from increased oxidative stress in aging tissues contributes to mitochondrial dysfunction in aging and disease (Harman 1972; Harper et al. 2004; Jang et al. 2010). Mitochondria generate reactive oxygen species (ROS) in the form of superoxide anion at complexes I and III of the electron transport chain (ETC) as a normal byproduct of aerobic metabolism (St-Pierre et al. 2002; Jackson et al. 2007). As a result of their proximity to the ETC, mitochondrial proteins, lipids, and DNA incur significant oxidative damage. In skeletal muscle, evidence suggests that oxidative damage to mitochondria is linked to reduced oxidative phosphorylation capacity (Papa 1996), degeneration of neuromuscular junctions (Jang et al. 2010), and apoptosis (Pollack et al. 2002).

Periods of elevated oxidative stress are a normal part of physiological processes. For example, mitochondrial ROS production is elevated following exercise (Anderson et al. 2007) and during high fat feeding (Anderson et al. 2009). Consequently, mitochondria have evolved intrinsic antioxidant defense mechanisms to maintain redox homeostasis. One such proposed mechanism is ROS-induced uncoupling of oxidative phosphorylation, whereby oxidative stress activates pathway(s) which dissipate the mitochondrial inner membrane (MIM) potential without generating ATP (Skulachev 1996; Brand 2000; Echtay et al. 2002), leading to a reduction in the ATP produced per oxygen atom consumed by the ETC (lower P/O). ROS production by the ETC is driven by a high MIM potential (Korshunov et al. 1997) due mainly to the slowed passage of electrons through complexes I and III leading to increased probability for the partial reduction of O_2 (Nicholls 2004). Mild uncoupling increases electron flux through the ETC for a given rate of ATP production and causes a reduction in ROS production at the cost of reduced energetic efficiency. Evidence for this negative feedback hypothesis comes from recent work demonstrating that increased oxidative stress results in reduced in vivo P/O in skeletal muscle (Siegel et al. 2011), and studies suggesting that mitochondrial uncoupling is protective against age-related dysfunction (Amara et al. 2007) and associated with increased lifespan (Speakman et al. 2004; Caldeira da Silva et al. 2008; Andrews 2010).

Despite the importance of ROS-induced uncoupling in maintaining redox homeostasis, little is known about the effect of aging on ROS-induced uncoupling. Age-related decreases in mitochondrial P/O and phosphorylation capacity (Conley et al. 2000; Marcinek et al. 2005; Amara et al. 2007) suggest that the flexibility of mitochondria to further uncouple in response to changing intracellular environments may be compromised. The diminishing utility of this defense mechanism with age would represent a significant loss of an antioxidant defense and may contribute to the age-related buildup of oxidative damage. Furthermore, the link between ROS-induced uncoupling and cellular energetics may present a unique challenge to old organisms that are already struggling to maintain energy balance (Wilson and Morley 2003; Marcinek et al. 2005; Amara et al. 2007).

Here we test the hypothesis that age-related deficiencies in mitochondrial function disrupt the ROS-induced uncoupling mechanism, rendering old skeletal muscle less able to adapt to transient increases in oxidative stress. To address this hypothesis we introduce a novel multi-modal in vivo spectroscopy system capable of acquiring simultaneous magnetic resonance (MR) spectra and near infrared (NIR) optical spectra from skeletal muscle in the fully intact mouse hindlimb. We use a mild paraquat (PQ) treatment to induce an acute oxidative insult in mice at young, middle, and old ages to measure the effect of age on the ability of skeletal muscle mitochondria to adapt to this insult in vivo. PQ is a redox cycling agent leading to increased production of superoxide at both cytosolic and mitochondrial

NAD(P)H oxidases (Cocheme and Murphy 2008). We use UCP3 knockout mice to test whether the activation of UCP3 mediated proton leak is responsible for PQ-related changes in in vivo P/O observed in this study.

2. Methods

2.1 Animals

This study was approved by the Institutional Animal Care and Use Committee of the University of Washington. For aging studies, young (5-7 months), middle aged (20-21 months), and old (27-28 months) female C57BL/6 mice were purchased from the aged mouse colony maintained by the NIA at Charles River Laboratories (Wilmington, MA). Female $UCP3^{-/-}$ mice on a C57BL/6J background (Gong et al. 2000) were studied between 4 and 7 months of age. All mice were kept on a 12 hour light/dark cycle at 22°C and 20% humidity with free access to water and standard mouse chow until immediately prior to experimentation. Mice were warmed using forced air to maintain skeletal muscle temperature at 36°C ± 1° throughout in vivo experiments.

2.2 Paraquat

Paraquat (Item 36541, Sigma, St. Louis, MO) was dissolved in 0.9% filtered saline at a concentration of 1mg/mL and administered by intraperitoneal injection. Mice received either 20mg PQ per kg of body weight or volume matched saline on the evening prior to in vivo experiments.

2.3 Multi-Modal Spectroscopy

Mice were anesthetized by intraperitoneal injection of 0.01ml/g of 2.5% tribromoethanol (“Avertin”, Sigma) and the left distal hindlimb shaved using veterinary hair clippers. As illustrated in Fig. 1, mice were then suspended using Velcro straps in a custom built MR/optics probe. We developed custom probes for use with either 7T (Varian, Palo Alto, CA) or 14T (Bruker, Billerica, MA) vertical bore spectrometers. Both probes employed the same general design: the distal hindlimb is centered within a horizontal, solenoid MR coil tunable to both ^{1}H and ^{31}P with the foot fixed against a plastic post. Aligned fiber optic bundles are positioned on either side of the coil (perpendicular to the coil axis), to deliver light from a QTH source (Newport Corp, Irvine, CA) to the lateral surface of the distal hindlimb, collect light transmitted through the hindlimb, and deliver this transmitted light to a spectrograph coupled to a CCD camera (Princeton Instruments, Trenton, NJ). A custom-built, inflatable ischemia cuff was positioned around the hindlimb proximal to the MR/optics hardware so that blood flow to the distal hindlimb could be rapidly blocked and restored with an external sphygmomanometer during in vivo experiments. Complete short term ischemia is used to perturb the energy homeostasis in the skeletal muscle for measurement of mitochondrial ATP and O_2 fluxes (Blei et al. 1993; Marcinek et al. 2004).

After positioning the mouse, MR signal was optimized by shimming the ^{1}H peak using tissue water and optical signal was optimized by adjusting acquisition time (typically 30-60ms). A high signal to noise ^{31}P spectrum was acquired under fully relaxed conditions (32 transients, 4096 complex points, 10kHz sweep width, 25s interpulse delay at 7T; 80 transients, 8192 complex points, 20kHz sweep width, 10s interpulse delay at 14T). Dynamic optical (0.5s delay) and MR spectra (45° flip angle, 4 transients, 4096 complex points, 10kHz sweep width, 1.5s interpulse delay, at 7T; 45° flip angle, 4 transients, 4096 complex points, 20kHz sweep width, 0.6s interpulse delay at 14T) were acquired continuously through periods of rest (2min), ischemia (11min), and recovery (7min). After the first minute of rest mice breathed 100% O_2 for the remainder of each experiment. Experiment timing is summarized in Fig. 2. Spectra acquired using 7T and 14T systems were similar

(Fig. S1) and flux rates and metabolite concentrations acquired on the two systems were not different.

2.4 Tissue Preparation

Immediately following in vivo spectroscopy, mice were injected with a supplemental, non-lethal dose of Avertin and the skeletal muscles of the distal hindlimb were dissected and flash-frozen in liquid nitrogen. From the left leg, extensor digitorum longus, gastrocnemius, soleus, and tibialis anterior muscles were pooled and pulverized over liquid nitrogen for measurement of mixed muscle metabolite, hemoglobin (Hb), and myoglobin (Mb) concentrations. From the right leg, gastrocnemius was pulverized over liquid nitrogen and prepared for western blotting. All muscle samples were stored at -80° until the day of assay.

2.5 Metabolite Concentrations

Tissue concentrations of ATP and total creatine (Cr) were determined in mixed muscle by HPLC (Waters, Milford, MA) using a protocol described in detail elsewhere (Wiseman et al. 1992).

2.6 Protein Content

Absolute Hb and Mb concentrations were determined using Coomassie-staining with in-gel standards of known concentration. Aliquots of pulverized mixed muscle were combined 1:25 with Cellytic MT lysis buffer (Sigma #C3228) containing 0.1% protease inhibitor (Sigma #P8340), and homogenized at 4°C using a Bullet Blender 24 (Next Advance, Averill Park, NY). The resulting lysate was combined 1:1 with tricine sample buffer (Bio-Rad #161-0739) containing 350mM DTT and brought to 95°C for 8 minutes. Proteins were separated on 10-20% gradient gels at 150V for 2.5 hours and then stained overnight in Coomassie Brilliant Blue stain (Bio-Rad). After destaining, gels were imaged using the Bio-Rad ChemiDoc imaging system and band intensities were analyzed using QuantityOne software (Bio-Rad).

All other protein analyses were accomplished using western blotting. Aliquots of pulverized gastrocnemius were combined 1:25 with lysis buffer containing 0.1% protease inhibitor (same as above) plus 1% phosphatase inhibitor (Thermo Scientific #78420), and homogenized at 4°C using a Bullet Blender 24. The resulting lysate was combined 1:1 with Laemmli sample buffer (Bio-Rad #161-0737) containing 350mM DTT and proteins were separated on 4-20% gradient gels at 200V for 65-75 minutes. Proteins were transferred to nitrocellulose membranes, Ponceau stained to ensure uniform transfer and loading, and then immunoblotted as follows (block, primary, secondary): UCP3 (3%BSA 1hr at RT, 1:1K AbCam #3477 overnight at 4°, 1:10K Cell Signaling #7074 2hr at RT), ANT1 (5%BSA overnight at 4°, 1:1K Sigma #SAB2105530 2hr at RT, 1:5K Cell Signaling #7074 2hr at RT), ETC Complexes I-V (3%BSA 1hr at RT, 1:1K MitoSciences #604 overnight at 4°, 1:10K Cell Signaling #7076), HNE (5%NFDM 1hr at RT, 1:1K Alpha Diagnostics #HNE12s, 1:2K Alpha Diagnostics #30220). All antibodies were diluted in 1%BSA, except HNE for which 1%NFDM was used, and all solutions were made in 0.1% TTBS. When possible, α-tubulin (1:1K Cell Signaling #2125) was probed simultaneously as a loading control. When α-tubulin could not be probed due to target band overlap, Bradford assays were used to determine volume of total loaded protein. Membranes were developed using Immun-Star Western C Chemiluminescence Kits (Bio-Rad), imaged using a ChemiDoc imaging system, and band densities measured using QuantiyOne.

2.7 Multi-Modal Spectroscopy Data Analysis

^{31}P MR spectra were exponentially multiplied (20Hz at 7T, 40Hz at 14T), Fourier transformed, and manually phase corrected using Varian VNMR (7T) or Bruker TopSpin (14T) software. The resulting spectra were taken to custom written MATLAB software (Mathworks, Natick, MA) for the remainder of analysis. Raw optical spectra files collected using WinSpec (Princeton Instruments) were taken directly to custom written MATLAB software for analysis.

The method used for analyzing MR spectra is described in detail elsewhere (Marcinek et al. 2004). Relative peak integrals from fully relaxed ^{31}P MR spectra were used to calculate the resting inorganic phosphate (P_i) /ATP and PCr/ATP ratios. After summing 3 consecutive dynamic spectra to improve signal-to-noise ratio, we used the Fit-to-Standard algorithm (Heineman et al. 1990) to determine PCr and P_i peak magnitudes throughout dynamic acquisition, relative to rest. After correcting for variable relaxation, the ATP concentration from HPLC analysis of mixed muscle was used as an internal reference to calculate absolute PCr and P_i concentrations over time. pH was determined using the chemical shift between P_i and PCr peaks, and ADP and AMP concentrations were calculated using the known kinetics of the creatine kinase and adenylate kinase reactions, assuming equilibrium conditions and a Mg^{2+} concentration of 0.6mM (Taylor et al. 1983; Golding et al. 1995; Kushmerick 1997).

The method used for analyzing optical spectra has been described in detail previously (Marcinek et al. 2004). After taking the second-derivative of optical spectra to minimize the influence of tissue scattering, we used a partial least squares (PLS) routine to determine the O_2 saturations of Hb and Mb throughout dynamic spectral acquisition (Arakaki et al. 2007). The O_2 saturation values and concentrations of Hb and Mb were used to determine the change in tissue O_2 stores during ischemia according to:

$$MO_2 = \Delta\left(Hbsat \times [Hb] + PO_{2vasc} \times O_2sol + Mbsat \times [Mb] + PO_{2cell} \times O_2sol\right)/\Delta t \quad \text{(eq. 1)}$$

where MO_2 is the oxygen consumption rate in $\mu mol(g*s)^{-1}$, [Hb] and [Mb] are expressed in $\mu mol\ g^{-1}$, PO_{2vasc} and PO_{2cell} are the partial pressures of oxygen in the vascular and intracellular compartments, respectively, and O_2sol is the solubility of oxygen (0.0014 $\mu mol\ O_2(ml\ mm\ Hg)^{-1}$) (Bentley et al. 1993). PO_{2vasc} and PO_{2cell} are calculated from the saturations of Mb and Hb using P_{50} values for Mb and Hb of 2.39 mm Hg (Schenkman et al. 1997) and 44 mm Hg (Schmidt-Neilsen and Larimer 1958), respectively.

The resting rates of mitochondrial ATP production (ATPase) and O_2 consumption were calculated during ischemia from least-squares linear approximations of the decline in PCr (Phase C, Fig. 3) and O_2 (Phase B, Fig. 3), respectively. Phase C represents the period of alkalinization where there no increase in the rate of glycolytic ATP production to confound our measurement of PCr breakdown (Conley et al. 1997). We have recently confirmed this for the ischemic protocol in mouse skeletal muscle by comparing lactate accumulation with MR analyses of glycolytic rate (Marcinek et al. 2010). Thus, during this period the rate of PCr breakdown is equivalent to the mitochondrial ATP production under normoxic conditions (Marcinek et al. 2004). O_2 consumption is determined during the first part of Phase B before Mb O_2 saturation drops to 50% and intramuscular O_2 tension becomes rate-limiting to oxidative phosphorylation (Marcinek et al. 2003). These resting rates of mitochondrial ATP and O_2 fluxes are used to calculate the in vivo P/O (0.5 × ATPase/O_2 consumption). The maximum rate of oxidative phosphorylation (ATPmax) was calculated using a least-squares monoexponential approximation of PCr synthesis during recovery from ischemia (Blei et al. 1993), beginning from the time at which a least-squares hyperbolic fit of Mb O_2 saturation had recovered to 50%.

2.8 Statistics

Statistical analysis was carried out using Prism 5 software (GraphPad, La Jolla, CA). Based on a priori hypotheses for measurements of energetic parameters, one-tailed student's t-tests were used to compare PQ-treatment vs. control at every age and middle aged and old controls vs. young controls. Two-tailed student's t-tests were used for analyses of protein expression data. t-tests were chosen over analysis of all age groups with linear regression because it makes fewer assumptions and provides unambiguous comparisons. The boundary for statistical significance was set at $p = 0.05$.

3. Results

3.1 Multi-modal spectroscopy is a novel method for measuring in vivo energetics

To measure in vivo mitochondrial metabolism in mouse skeletal muscle during a single experiment we used a novel combined MR and optical spectroscopy system. As illustrated in Fig. 1A, the distal hindlimb of an anesthetized mouse is passed through an inflatable ischemia cuff and positioned in the center of a horizontal MR coil, which is flanked on either side by fiber optic bundles. We use this setup to simultaneously collect ^{31}P-MR spectra and NIR optical spectra during periods of rest, brief ischemia, and recovery (Fig. 2). The changes in MR and optical spectra during this protocol are illustrated in Figs. 1B and 1C, respectively. As described previously, optical spectra can be used to measure the rate at which O_2 is consumed as the terminal electron acceptor of oxidative phosphorylation (Marcinek et al. 2004), and ^{31}P-MR spectra can be used to quantify the rate of mitochondrial ATP production (Blei et al. 1993).

By acquiring MR and optical spectra simultaneously we are able to measure acute metabolic changes in vivo and to make time-resolved comparisons between the O_2 saturations of Hb and Mb, phosphometabolite concentrations, and pH (illustrated and discussed in Fig. 3).

3.2 Aged mitochondria uncouple in response to oxidative insult despite pre-existing inefficiency

We used in vivo spectroscopy to measure the efficiency of mitochondrial oxidative phosphorylation (ATP produced per oxygen atom consumed; P/O ratio) in young (5-7 months), middle aged (21-22 months), and old (27-28 months) C57BL/6 mice with a published median lifespan of 26 months (Turturro et al. 1999). To test the hypothesis that ROS-induced uncoupling is diminished with age, mice received intraperitoneal injections of either 20mg/kg PQ or volume-matched saline (C) one day prior to in vivo spectroscopy to elevate mitochondrial and cytosolic superoxide production (Cocheme and Murphy 2008). This low dose of PQ was chosen well below the LD_{50} of 70mg/kg to induce an acute period of mildly elevated ROS production (Drew and Gram 1979). The mild nature of the PQ-induced oxidative insult was confirmed as an age, but not PQ, related increase of 4-hydroxy-2-nonenal (HNE) protein adducts in gastrocnemius muscle (Fig. S2).

Consistent with previous reports in mice and humans (Marcinek et al. 2005; Amara et al. 2007), P/O ratio declined with age. Despite this age-related loss of mitochondrial efficiency, P/O decreased in response to PQ treatment at all three ages (Fig. 4A). In all cases, a significant decrease in mitochondrial ATPase rate with insignificant trends toward faster O_2 consumption (Figs. 4B and 4C) was responsible for decreases in P/O. The relative magnitude of PQ-induced uncoupling was not lost with age (34% for young, 22% for middle aged, and 34% for old), despite the significantly lower resting P/O in aged mice. As a result, the P/O ratio in old PQ-treated mice was 50% lower than that of untreated young mice.

3.3 Mitochondrial uncoupling with PQ-treatment is independent of UCP3 in vivo

To test the hypothesis that activation of proton leak through UCP3 was responsible for the decreases in P/O ratio that we observed, we first measured UCP3 protein content in gastrocnemius from mice in all six age/treatment groups. Confirming previous results, UCP3 protein expression decreased significantly with age (Kerner et al. 2001) and was unaffected by PQ treatment (Siegel et al. 2011) (Fig. 5), suggesting that the magnitude of uncoupling was unaffected by UCP3 protein levels. Protein expression of another putative uncoupler of oxidative phosphorylation in skeletal muscle, ANT1, was not different with age or PQ-treatment (Fig. S3).

To further test the role of UCP3 in ROS-induced uncoupling, we measured the effects of PQ treatment on in vivo P/O ratio in young $UCP3^{-/-}$ mice. PQ-treatment induced a significant drop in P/O ratio in $UCP3^{-/-}$ mice of the same magnitude observed in wild-type mice used for the aging experiments (mean difference of 29%, Fig. 6). The absence of UCP3 protein was verified in mixed skeletal muscle of $UCP3^{-/-}$ mice by western blot (Fig. S4).

3.4 Acute oxidative insult reduces in vivo phosphorylation capacity in old mice only

The rate of recovery of PCr from ischemia provides a measure of the maximum rate of oxidative phosphorylation (ATPmax, Fig. 3) (Blei et al. 1993). Using the monoexponential time constant of PCr recovery from the time at which a hyperbolic fit of Mb saturation recovered to 50% we eliminated a significant dependence of PCr recovery kinetics upon the rate of muscle reperfusion (Fig. S5).

In old mice, ATPmax was approximately 30% lower than young controls and declined even further with PQ treatment (Fig. 7A). In contrast, ATPmax was not affected by age or PQ treatment in young and middle aged mice. Using western blot analysis of mixed gastrocnemius, we tested the hypothesis that the decreases in ATPmax were due to reduced expression of ETC proteins. Protein expression of ETC complexes I-V actually increased significantly with age and we observed no significant effect of PQ (Fig. S6).

3.5 Acute oxidative insult disrupts energy homeostasis in aged mice

We measured metabolite concentrations in resting skeletal muscle to determine the effects of changes in mitochondrial function on muscle energetics in vivo (Table 1). As depicted in Fig. 7B, ATP concentration was unaffected by PQ-treatment in young mice and was maintained in middle aged controls. However, ATP was significantly lower in old mice and decreased in response to PQ treatment in both middle aged and old mice. In PQ-treated young and middle aged mice, PCr/ATP decreased and AMP/ATP increased, indicative of energetic stress associated with decreased P/O. However, PCr/ATP and AMP/ATP ratios were insensitive to PQ treatment in old mice. We also observed significant losses of PCr and Cr in old vs. young mice, and an increase in resting pH in old mice that was significantly reduced by PQ-treatment.

4. Discussion

This study tests the ability of aged mitochondria to functionally adapt to an acute oxidative insult induced by PQ-treatment. Contrary to our initial hypothesis, mitochondrial uncoupling in response to oxidative insult persisted between the ages of 5 and 28 months in mouse skeletal muscle. Interestingly, this insult resulted in deficits in mitochondrial ATPmax and ATP concentration in old mice only. These results provide novel insight into the effects of oxidative stress on metabolic function throughout life and reveal reduced adaptability of aged mitochondria to mild physiological stress. Using $UCP3^{-/-}$ mice we demonstrate that this PQ-induced in vivo uncoupling is independent of UCP3 in skeletal muscle.

4.1 In vivo spectroscopy

MR (Kemp et al. 2007; Forbes et al. 2009; Jeneson et al. 2009; Lanza et al. 2010) and optical (Schenkman et al. 1999; Arakaki et al. 2007; Murkin and Arango 2009) spectroscopy are powerful methods for measuring tissue energetics and oxygenation state. Due to the interaction between tissue oxygenation state and mitochondrial energetics it is important to measure both parameters to understand the effects of a perturbation on skeletal muscle metabolism. For the current study we developed an integrated MR and optical spectroscopy system for use with mouse models of disease (Fig. 1) to make simultaneous time-resolved measurements of both energetics and oxygenation using a short ischemic protocol. This represents an important progression from previous work using separately acquired MR and optical spectra to measure skeletal muscle energetics in humans (Amara et al. 2008) and mice (Marcinek et al. 2004). Mitochondrial ATP and O_2 fluxes and P/O values reported here are consistent with those obtained using separate measurements of MR and optical spectroscopy (Marcinek et al. 2004) and with independent ex vivo methods (Paul and Kushmerick 1974; Kingsley-Hickman et al. 1987; Sako et al. 1988). Here we demonstrate the power of the simultaneous measurement of MR and optical spectroscopy for measuring the effects of age on the metabolic response to acute oxidative insult in vivo.

In vivo measurements of mitochondrial coupling efficiency (P/O) and phosphorylation capacity (ATPmax) are both improved by simultaneous acquisition of MR and optical spectra. First, by performing a single experiment lasting less than one hour, we are able to measure mitochondria responding to acute changes in the intracellular environment. Second, by aligning measurements of PCr concentration and pH with measurements of O_2 saturations of Hb and Mb we are able to identify the time boundaries between which glycolysis and intracellular O_2 tension do not affect the rates of PCr hydrolysis or PCr synthesis (Fig. 3). The benefit of this ability is illustrated in Fig. S5, which demonstrates that calculating ATPmax from the point at which muscle reperfusion has elevated Mb saturation to 50% eliminates an oxygen limitation to muscle PCr recovery kinetics.

4.2 ROS-induced uncoupling in vivo

We have previously shown that an oxidative insult to mouse skeletal muscle results in in vivo uncoupling, independent of intrinsic changes to the mitochondria (Siegel et al. 2011). This uncoupling suggests an increase in proton leak associated with a reduction in MIM potential and a decrease in mitochondrial ROS production (Skulachev 1996; Brand 2000; Echtay et al. 2002). Consistent with previous reports in both mice (Marcinek et al. 2005) and humans (Amara et al. 2007) we find that aging is associated with declines in resting mitochondrial P/O and ATP levels in skeletal muscle. The current study demonstrates that, despite these mitochondrial deficits in aged muscle, ROS-induced uncoupling persists into old age (Fig. 4A). As a result, downstream energetic consequences of decreased P/O (approximately 50% decrease in old PQ-treated mice relative to young controls) indicate a greater disruption of cell metabolism due to acute mild oxidative insult in aged mice. It remains to be determined if the mechanisms underlying the reduced P/O in response to PQ differ in old and young skeletal muscle.

4.3 UCP3

The role of UCP3 in ROS-induced uncoupling in vivo remains uncertain. Uncoupling proteins can be activated by ROS or by-products of lipid peroxidation to increase proton leak across the MIM in vitro (Echtay 2007). Mailloux, et al. recently demonstrated that UCP3 mediated proton leak in situ was acutely controlled by the glutathionylation of UCP3, which was sensitive to the redox state of the mitochondria (Mailloux et al. 2011). However, our results indicate that UCP3 does not contribute to the PQ-induced uncoupling in vivo observed in this study.

Despite lacking UCP3, skeletal muscle mitochondria in young adult UCP3$^{-/-}$ mice exhibited decreased P/O one day after PQ treatment. The magnitude of this uncoupling was similar to the magnitude of uncoupling observed in our aging study indicating that reduced in vivo P/O one day after PQ-treatment observed in this study are independent of UCP3. Recent data suggest a model in which UCPs are activated and deactivated by fluctuations in the redox environment of the mitochondria on the order of one or two minutes, but longer increases in oxidative stress deactivate UCP3 to preserve mitochondrial membrane potential (Toime and Brand 2010; Mailloux and Harper 2011). Since our measurements were made one day after PQ treatment our results in UCP3$^{-/-}$ mice do not preclude a role for UCP3 in ROS-induced uncoupling on this shorter time scale or in response to other types of ROS.

Another putative uncoupler in skeletal muscle mitochondria, ANT1, represents a possible alternative conduit for ROS-induced uncoupling (Bevilacqua et al. 2010). The quantity of ANT1 is expected to be more than 500-fold greater than that of UCP3 (Harper et al. 2002; Brand et al. 2005) and we detected constant levels of ANT1 regardless of age or PQ-treatment (Fig. S3). As a result, ANT1 mediated proton leak remains a potential mechanism to explain the reduced P/O with PQ treatment in skeletal muscle in vivo. In addition, other anion carriers use the MIM proton gradient to drive transport of metabolites across the MIM (Brand et al. 2005). Changes in the activity of these transporters may also contribute to the dissipation of the proton gradient and result in reduced in vivo P/O in response to mild oxidative stress.

4.4 Effects of ROS-induced uncoupling on downstream energetics

Mitochondrial phosphorylation capacity (ATPmax) represents the capacity for oxidative phosphorylation to meet increases in cellular ATP demand beyond the resting rate (ATPase). In mice, values for ATPmax are approximately 30 times greater than resting ATPase rate in vivo (Siegel et al. 2011) indicating that the capacity for ATP synthesis far exceeds the ATP demand under resting conditions. However, under non-resting conditions (like contraction in the case of skeletal muscle), the rate of cellular ATP demand can increase several fold and exceed mitochondrial phosphorylation capacity. Thus, loss of this reserve functional capacity resulting from reduction of ATPmax can lead to decreased fatigue resistance and impaired function.

ATPmax was significantly lower in the oldest mice, despite an increase in ETC complex protein expression in the gastrocnemius muscle (Fig. S6). This reduced capacity/content is consistent with previous reports in vivo in humans (Conley et al. 2000) and ex vivo in rodents (Picard et al. 2011) and could be due to decreased mitochondrial quality control and accumulation of oxidative damage to mitochondrial DNA and protein (Cortopassi et al. 1992; Li et al. 2012). Although different from the conventional view of reduced mitochondrial content with age, the increase in mitochondrial proteins in this study is consistent with a recent report from predominantly glycolytic muscle in aged rats (Picard et al. 2011) and demonstrates the tissue heterogeneity of the effects of age on mitochondria.

Interestingly, PQ-treatment resulted in a significant decrease in ATPmax in old mice only. The relative change in ATPmax is in almost perfect agreement with the drop in P/O ratio in both old control (25% ΔP/O, 28% ΔATPmax) and old PQ-treated (50% ΔP/O, 49% ΔATPmax) mice relative to young controls, suggesting that ROS-induced uncoupling is a significant contributor to the loss of capacity in both instances. This is contrary to results in young and middle aged mice in which changes in efficiency are insignificant at maximal rates of flux thus preserving the capacity for mitochondrial ATP production at higher flux rates. This loss of capacity represents a unique deficiency in old mice that indicates old mitochondria exist at the edge of an energetic threshold beyond which normal physiological fluctuations have significant consequences on reserve capacity for ATP production.

Intracellular ATP concentration is another measure of the ability of skeletal muscle mitochondria to maintain energy homeostasis. PQ-treatment led to drops in ATP content in middle aged and old, but not young, mice (Fig. 7B). Under normal conditions, ATP is buffered by the activities of the creatine kinase and adenylate kinase reactions in skeletal muscle (Kushmerick 1998). As a result, mismatches between ATP production and ATP demand (in this case, a decrease in P/O caused by ROS-induced uncoupling) manifest as decreases in PCr/ATP and increases in AMP/ATP ratios while ATP remains constant. Net loss of ATP only occurs under conditions of severe energy stress when a chronically elevated AMP/ATP ratio leads to net loss of adenosine via enzymatic purine catabolism (Sutton et al. 1980). Our results indicate that young mice are able to maintain energy homeostasis during ROS-induced uncoupling, while older mice enter a more severe state of energy stress that results in net loss of ATP.

We observed additional unique differences in resting metabolite concentrations in aging skeletal muscle (Table 1). Similar to previous reports (Marcinek et al. 2005; Amara et al. 2007), PCr and Cr decreased alongside reductions in ATP with age and/or PQ-treatment. This may be indicative of adaptation to chronic alterations in the resting metabolite profile, or may result from increased muscle damage and fibrosis in the aged muscle leading to artificially depressed concentration measurements. Also, under resting conditions, pH was significantly elevated in old animals and, unlike any other age group, pH decreased in response to PQ-treatment. Intracellular pH can be used to measure glycolytic activity (Marcinek et al. 2010), so this might suggest decreased reliance on substrate-level phosphorylation in old muscle that becomes more active in response to oxidative stress. However, our experiments were not designed to quantify glycolytic activity and a relationship between resting pH and glycolysis has not been established (Crowther et al. 2002). Future studies using in vivo MR spectroscopy should address this phenomenon directly.

4.5 Significance and Conclusions

Aged mitochondria maintain the capacity to respond to acute changes in the oxidative environment but lack the ability to maintain energy homeostasis in response to the induced changes in mitochondrial energetics. This loss of energy homeostasis in response to mild physiological stress may contribute to loss of function and degeneration of skeletal muscle with age.

Supplementary Material

Refer to Web version on PubMed Central for supplementary material.

Acknowledgments

We thank Gary Knowels, Dr. Shane Kruse, and Rudolph Stuppard for their technical assistance and Dr. Mary Emond for her statistical consultation. This work was supported by NIH grants AG028455, AG036606, and AG001751 and a New Scholar Award from the Ellison Medical Foundation.

Abbreviations

ANT1	Adenine Nucleotide Translocase 1
ATPase	Resting rate of ATP hydrolysis
ATPmax	Maximum rate of oxidative phosphorylation
Cr	Total Creatine

ETC	Electron Transport Chain
FDI	First Dorsal Interosseous
Hb	Hemoglobin
HNE	4-hydroxy-2-nonenal
Mb	Myoglobin
MIM	Mitochondrial Inner Membrane
MR	Magnetic Resonance
NIR	Near-Infrared
PLS	Partial Least Squares
PCr	Phosphocreatine
P_i	Inorganic Phosphate
P/O	ATP produced per oxygen atom consumed
PQ	Paraquat
ROS	Reactive Oxygen Species
UCP3	Uncoupling Protein 3

References

Amara C, Marcinek D, et al. Mitochondrial function in vivo: Spectroscopy provides window on cellular energetics. Methods. 2008; 46(4):312–318. [PubMed: 18930151]

Amara C, Shankland E, et al. Mild mitochondrial uncoupling impacts cellular aging in human muscles in vivo. Proceedings of the National Academy of Science. 2007; 104(3):1057–1062.

Anderson E, Lustig M, et al. Mitochondrial H2O2 emission and cellular redox state link excess fat intake to insulin resistance in both rodents and humans. The Journal of Clinical Investigation. 2009; 119(3):573–581. [PubMed: 19188683]

Anderson E, Yamazaki H, et al. Induction of Endogenous Uncoupling Protein 3 Suppresses Mitochondrial Oxidant Emission during Fatty Acid-supported Respiration. The Journal of Biochemistry. 2007; 282(43):31257–31266.

Andrews ZB. Uncoupling protein-2 and the potential link between metabolism and longevity. Curr Aging Sci. 2010; 3(2):102–112. [PubMed: 20158496]

Arakaki L, Burns D, et al. Accurate Myoglobin Oxygen Saturation by Optical Spectroscopy Measured in Blood-Perfused Rat Muscle. Applied Spectroscopy. 2007; 61(9):978–985. [PubMed: 17910795]

Bentley TB, Meng H, et al. Temperature dependence of oxygen diffusion and consumption in mammalian striated muscle. American Journal Physiology. 1993; 264(33):H1825–H1830.

Bevilacqua L, Seifert E, et al. Absence of uncoupling protein-3 leads to greater activation of an adenine nucleotide translocase-mediated proton conductance in skeletal muscle mitochondria from calorie restricted mice. Biochimica et Biophysica Acta. 2010; 1797(8):1389–1397. [PubMed: 20206124]

Blei ML, Conley KE, et al. Separate measures of ATP utilization and recovery in human skeletal muscle. The Journal of Physiology. 1993; 465(1):203–222. [PubMed: 8024651]

Brand M. Uncoupling to survive? The role of mitochondrial inefficiency in ageing. Experimental Gerontology. 2000; 35:811–820. [PubMed: 11053672]

Brand MD, Pakay JL, et al. The basal proton conductance of mitochondria depends on adenine nucleotide translocase content. Biochem J. 2005; 392(Pt 2):353–362. [PubMed: 16076285]

Caldeira da Silva CC, Cerqueira FM, et al. Mild mitochondrial uncoupling in mice affects energy metabolism, redox balance and longevity. Aging Cell. 2008; 7(4):552–560. [PubMed: 18505478]

Cocheme H, Murphy M. Complex I Is the Major Site of Mitochondrial Superoxide Production by Paraquat. The Journal of Biological Chemistry. 2008; 283(4):1786–1798. [PubMed: 18039652]

Conley K, Jubrias S, et al. Oxidative capacity and ageing in human muscle. Journal of Physiology. 2000; 526(1):203–210. [PubMed: 10878112]

Conley KE, Blei ML, et al. Activation of glycolysis in human muscle in vivo. American Journal of Physiology - Cell Physiology. 1997; 273(1):C306–C315.

Cortopassi GA, Shibata D, et al. A pattern of accumulation of a somatic deletion of mitochondrial DNA in aging human tissues. Proc Natl Acad Sci U S A. 1992; 89(16):7370–7374. [PubMed: 1502147]

Crowther G, Carey M, et al. The control of glycoloysis in contracting skeletal muscle. I. Turning it on. American Journal of Physiology. Endocrinology and Metabolism. 2002; 282(1):E67–E73. [PubMed: 11739085]

Drew R, Gram TE. Vehicle alteration of paraquat lethality in mice. Toxicol Appl Pharmacol. 1979; 48(3):479–487. [PubMed: 473191]

Echtay K. Mitochondrial uncoupling proteins - What is their physiological role? Free Radical Biology & Medicine. 2007; 43(10):1351–1371. [PubMed: 17936181]

Echtay K, Roussel D, et al. Superoxide activates mitochondrial uncoupling proteins. Nature. 2002; 415:96–99. [PubMed: 11780125]

Forbes SC, Paganini AT, et al. Phosphocreatine recovery kinetics following low- and high-intensity exercise in human triceps surae and rat posterior hindlimb muscles. American Journal of Physiology - Regulatory, Integrative and Comparative Physiology. 2009; 296(1):R161–R170.

Gibson GE, Starkov A, et al. Cause and consequence: Mitochondrial dysfunction initiates and propagates neuronal dysfunction, neuronal death and behavioral abnormalities in age-associated neurodegenerative diseases. Biochimica et Biophysica Acta (BBA) - Molecular Basis of Disease. 2010; 1802(1):122–134.

Golding E, Teague W, et al. Adjustment of K' to varying pH and pMg for the creatine kinase, adenylate kinase and ATP hydrolysis equilibria permitting quantitative bioenergetic assessment. J Exp Biol. 1995; 198(8):1775–1782. [PubMed: 7636446]

Gong D, Monemdjou S, et al. Lack of Obesity and Normal Response to Fasting and Thyroid Hormone in Mice Lacking Uncoupling Protein-3. The Journal of Biological Chemistry. 2000; 275(21): 16251–16257. [PubMed: 10748195]

Harman D. The biologic clock: the mitochondria? Journal of the American Geriatrics Society. 1972; 20(4):145–147. [PubMed: 5016631]

Harper JA, Stuart JA, et al. Artifactual uncoupling by uncoupling protein 3 in yeast mitochondria at the concentrations found in mouse and rat skeletal-muscle mitochondria. Biochem J. 2002; 361(Pt 1):49–56. [PubMed: 11743882]

Harper ME, Bevilacqua L, et al. Ageing, oxidative stress, and mitochondrial uncoupling. Acta Physiologica Scandinavica. 2004; 182(4):321–331. [PubMed: 15569093]

Heineman FW, Eng J, et al. NMR spectral analysis of kinetic data using natural lineshapes. Magn Reson Med. 1990; 13(3):490–497. [PubMed: 2325549]

Jackson MJ, Pye D, et al. The production of reactive oxygen and nitrogen species by skeletal muscle. Journal of Applied Physiology. 2007; 102(4):1664–1670. [PubMed: 17082364]

Jang Y, Lustgarten M, et al. Increased superoxide in vivo accelerates age-associated muscle atrophy through mitochondrial dysfunction and neuromuscular junction degeneration. The FASEB Journal. 2010; 24(5):1376–1390.

Jeneson JAL, Schmitz JPJ, et al. Magnitude and control of mitochondrial sensitivity to ADP. American Journal of Physiology - Endocrinology and Metabolism. 2009; 297(3):E774–E784. [PubMed: 19622784]

Kemp G, Meyerspeer M, et al. Absolute quantification of phosphorus metabolite concentrations in human muscle in vivo by 31P MRS: a quantitative review. NMR In Biomedicine. 2007; 20:555–565. [PubMed: 17628042]

Kerner J, Turkaly PJ, et al. Aging skeletal muscle mitochondria in the rat: decreased uncoupling protein-3 content. American Journal of Physiology - Endocrinology and Metabolism. 2001; 281(5):E1054–E1062. [PubMed: 11595663]

Kingsley-Hickman PB, Sako EY, et al. 31P NMR studies of ATP synthesis and hydrolysis kinetics in the intact myocardium. Biochemistry. 1987; 26(23):7501–7510. [PubMed: 3427090]

Korshunov SS, Skulachev VP, et al. High protonic potential actuates a mechanism of production of reactive oxygen species in mitochondria. FEBS Letters. 1997; 416(1):15–18. [PubMed: 9369223]

Kushmerick M. Energy balance in muscle activity: Simulations of ATPase coupled to oxidative phosphorylation and to creatine kinase. Comparative Biochemistry and Physiology Part B: Biochemistry and Molecular Biology. 1998; 120(1):109–123.

Kushmerick MJ. Multiple equilibria of cations with metabolites in muscle bioenergetics. American Journal of Physiology - Cell Physiology. 1997; 272(5):C1739–C1747.

Lang T, Streeper T, et al. Sarcopenia: etiology, clinical consequences, intervention, and assessment. Osteoporosis International. 2010; 21(4):543–559. [PubMed: 19779761]

Lanza IR, Tevald MA, et al. Intracellular energetics and critical Po2 in resting ischemic human skeletal muscle in vivo. American Journal of Physiology - Regulatory, Integrative and Comparative Physiology. 2010; 299(5):R1415–R1422.

Li X-D, Rebrin I, et al. Effects of age and caloric restriction on mitochondrial protein oxidative damage in mice. Mechanisms of Ageing and Development. 2012; 133(1):30–36. [PubMed: 22182424]

Mailloux RJ, Harper M-E. Uncoupling proteins and the control of mitochondrial reactive oxygen species production. Free Radical Biology and Medicine. 2011; 51(6):1106–1115. [PubMed: 21762777]

Mailloux RJ, Seifert EL, et al. Glutathionylation Acts as a Control Switch for Uncoupling Proteins UCP2 and UCP3. Journal of Biological Chemistry. 2011; 286(24):21865–21875. [PubMed: 21515686]

Marcinek D, Ciesielski W, et al. Oxygen regulation and limitation to cellular respiration in mouse skeletal muscle in vivo. Americal Journal of Physiology - Heart and Circulatory Physiology. 2003; 285(5):H1900–H1908.

Marcinek D, Kushmerick M, et al. Lactic acidosis in vivo: testing the link between lactate generation and H+ accumulation in ischemic mouse muscle. Journal of Applied Physiology. 2010; 108(6): 1479–1486. [PubMed: 20133437]

Marcinek D, Schenkman K, et al. Mitochondrial coupling in vivo in mouse skeletal muscle. The American Journal of Cell Physiology. 2004; 286:C457–C463.

Marcinek D, Schenkman K, et al. Reduced mitochondrial coupling in vivo alters cellular energetics in aged mouse skeletal muscle. Journal of Physiology. 2005; 569(2):467–473. [PubMed: 16254011]

Marzetti E, Leeuwenburgh C. Skeletal muscle apoptosis, sarcopenia and frailty at old age. Experimental Gerontology. 2006; 41(12):1234–1238. [PubMed: 17052879]

Murkin JM, Arango M. Near-infrared spectroscopy as an index of brain and tissue oxygenation. British Journal of Anaesthesia. 2009; 103(suppl 1):i3–i13. [PubMed: 20007987]

Nicholls D. Mitochondrial membrane potential and aging. Aging Cell. 2004; 3:35–40. [PubMed: 14965354]

Papa S. Mitochondrial oxidative phosphorylation changes in the life span. Molecular aspects and physiopathological implications. Biochimica et Biophysica Acta (BBA) - Bioenergetics. 1996; 1276(2):87–105.

Paul RJ, Kushmerick MJ. Apparent P-O ratio and chemical energy balance in frog sartorius muscle in vitro. Biochim Biophys Acta. 1974; 347(3):483–490. [PubMed: 4546275]

Picard M, Ritchie D, et al. Alterations in intrinsic mitochondrial function with aging are fiber type-specific and do not explain differential atrophy between muscles. Aging Cell. 2011; 10(6):1047–1055. [PubMed: 21933339]

Pollack M, Phaneuf S, et al. The Role of Apoptosis in the Normal Aging Brain, Skeletal Muscle, and Heart. Annals of the New York Academy of Sciences. 2002; 959(1):93–107. [PubMed: 11976189]

Sako EY, Kingsley-Hickman PB, et al. ATP synthesis kinetics and mitochondrial function in the postischemic myocardium as studied by ^{31}P NMR. Journal Biological Chemistry. 1988; 263(22): 10600–10607.

Schenkman K, Marble D, et al. Myoglobin oxygen dissociation by multiwavelength spectroscopy. Journal of Applied Physiology. 1997; 82(1):86–92. [PubMed: 9029202]

Schenkman K, Marble D, et al. Optical Spectroscopic Method for in Vivo Measurement of Cardiac Myoglobin Oxygen Saturation. Applied Spectroscopy. 1999; 53(3):332–338.

Schmidt-Neilsen K, Larimer JL. Oxygen Dissociation Curves of Mammalian Blood in Relation To Body Size. American Journal of Physiology -- Legacy Content. 1958; 195(2):424–428.

Siegel MP, Kruse SE, et al. Reduced Coupling of Oxidative Phosphorylation In Vivo Precedes Electron Transport Chain Defects Due to Mild Oxidative Stress in Mice. PLOS ONE. 2011; 6(11):e26963. [PubMed: 22132085]

Skulachev V. Role of uncoupled and non-coupled oxidations in maintenance of safely low levels of oxygen and its one-electron reductants. Quarterly Reviews of Biophysics. 1996; 29(2):169–202. [PubMed: 8870073]

Speakman J, Talbot D, et al. Uncoupled and surviving: individual mice with high metabolism have greater mitochondrial uncoupling and live longer. Aging Cell. 2004; (87-95)

St-Pierre J, Buckingham J, et al. Topology of Superoxide Production from Different Sites in the Mitochondrial Electron Transport Chain. The Journal of Biological Chemistry. 2002; 277(47): 44784–44790. [PubMed: 12237311]

Sutton JR, Toews CJ, et al. Purine metabolism during strenuous muscular exercise in man. Metabolism. 1980; 29(3):254–260. [PubMed: 7374440]

Taylor D, Bore P, et al. Bioenergetics of intact human muscle. A 31P nuclear magnetic resonance study. Molecular Biology & Medicine. 1983; 1(1):77–94. [PubMed: 6679873]

Toime L, Brand M. Uncoupling protein-3 lowers reactive oxygen species production in 3 isolated mitochondria. Free Radical Biology & Medicine. 2010; 49(4):606–611. [PubMed: 20493945]

Turturro A, Witt WW, et al. Growth curves and survival characteristics of the animals used in the Biomarkers of Aging Program. J Gerontol A Biol Sci Med Sci. 1999; 54(11):B492–501. [PubMed: 10619312]

Wilson M-MG, Morley JE. Invited Review: Aging and energy balance. Journal of Applied Physiology. 2003; 95(4):1728–1736. [PubMed: 12970378]

Wiseman R, Moerland T, et al. High-performance liquid chromatographic assays for free and phosphorylated derivatives of the creatine analogues beta-guanidopropionic acid and 1-carboxy-methyl-2-iminoimidazolidine (cyclocreatine). Analytical Biochemistry. 1992; 204(2):383–389. [PubMed: 1443539]

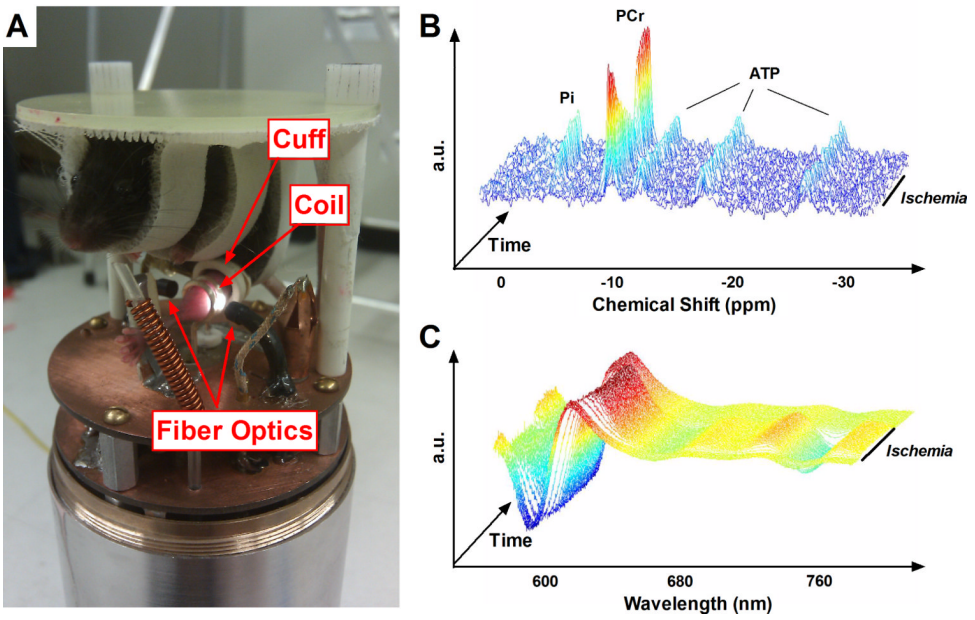

Fig. 1. Multi-modal in vivo spectroscopy

(A) Photograph of the combined MR and optical spectroscopy probe for use with the Bruker 14T spectrometer. An anesthetized mouse is suspended above spectroscopy hardware, with its shaved distal hindlimb positioned in the center of an MR coil tunable to both ^{1}H and ^{31}P, flanked on either side by fiber optic bundles. An inflatable ischemia cuff surrounds the hindlimb proximal to the MR coil. Unlabeled components visible in the picture include a 100% O_2 delivery line, thermocouple, and warm air delivery port. (B) Representative ^{31}P MR spectra (after exponential multiplication, Fourier transformation, and summing 5 consecutive spectra), stacked through the course of a dynamic in vivo experiment. During ischemia, PCr is broken down to maintain constant ATP as the resting energy demands of the cell are met and P_i undergoes a stoichiometric increase. (C) Representative NIR optical spectra (after taking second-derivative) during a dynamic in vivo experiment. As Hb and Mb deoxygenate during ischemia, a pronounced rightward shift is evident between ~580 and 660nm and a dramatic sinusoidal feature becomes prominent at ~760nm.

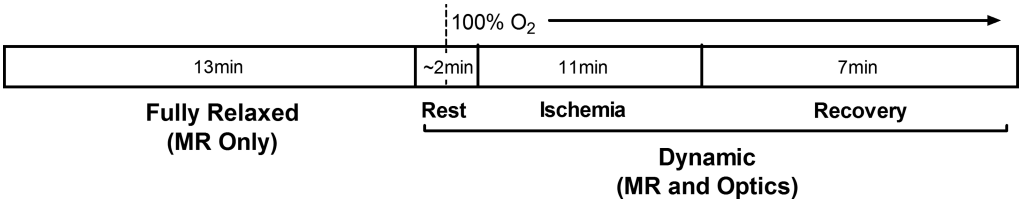

Fig. 2. Timeline for in vivo spectroscopy experiments

Timing of rest-ischemia-recovery during in vivo spectroscopy, corresponding with description in *Methods* section 2.3.

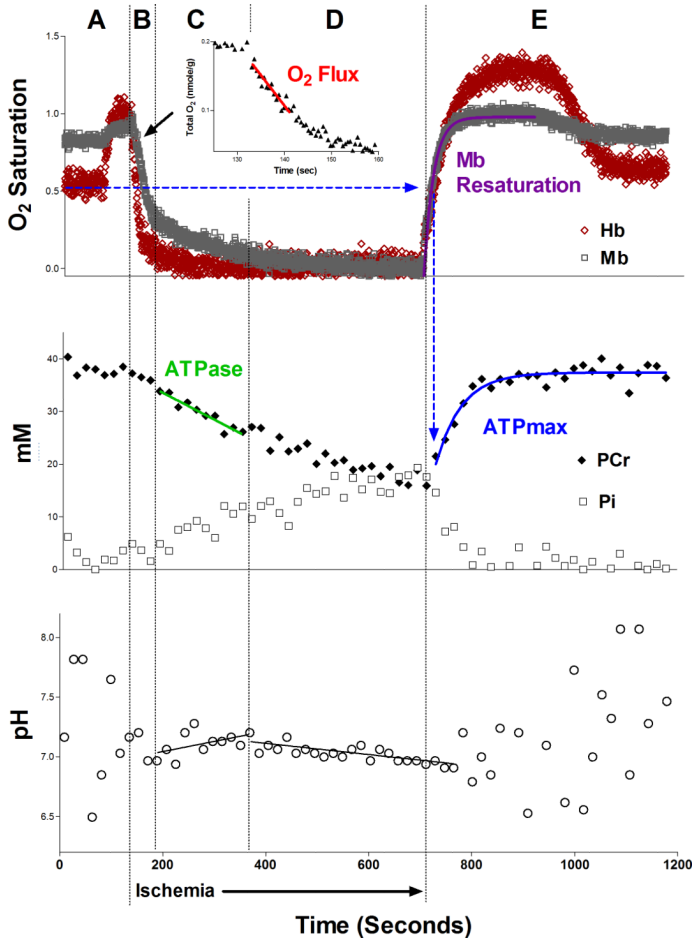

Fig. 3. Representative in vivo data

Representative time-course of Hb and Mb saturations (top), PCr and P_i concentrations (middle), and pH (bottom) following analysis of in vivo spectroscopy data. Distinct time-separated regions are identified by letters at the top and summarized as follows: (A) During an initial period of normal blood flow, delivery of 100% O_2 induces distinct increases in the O_2 saturations of Mb and Hb. During Phase A, PCr remains constant while oxidative phosphorylation meets ATP demand, and P_i is generally too low to overcome signal-to-noise limitations in mouse skeletal muscle. As a result pH measurements are not reliable during this time. (B) After inflating the ischemia cuff, O_2 that is bound to Hb and Mb in the now-closed system of the distal hindlimb is used to fuel oxidative phosphorylation for a short period of time. Thus, the rate of mitochondrial O_2 consumption ("O_2 Flux" in graph inset) can be measured using the rates of Hb and Mb desaturation. Low O_2 tension (below 50% Mb saturation (Marcinek et al. 2003)) begins to limit oxidative phosphorylation toward the end of Phase B. (C) Low intracellular O_2 tension inhibits oxidative phosphorylation and PCr is broken down to meet resting ATP demand. This is evident as linear changes in PCr (decrease) and P_i (increase), and a period of alkalinization accounted for by the proton stoichiometry of PCr hydrolysis (Marcinek et al. 2010). (D) As ischemia continues for up to 11 minutes, Hb and Mb become entirely deoxygenated. The rates of change of PCr and P_i slow down due to activation of glycolysis, which contributes to PCr synthesis. Due to this glycolytic activity, acidification is clear in a plot of pH vs. time. (E) Upon deflation of the ischemia cuff, muscle is reperfused leading to rapid recoveries of Hb and Mb saturations. PLS analysis of Mb saturation remains reliable during recovery, however measurement of

Hb saturation become unreliable at this point due to simultaneous changes in both Hb saturation and concentration. The rate of Mb resaturation can thus be used as a measure of the relative rate of muscle reperfusion. By measuring the monoexponential time constant of PCr recovery from the time at which Mb has recovered to 50%, illustrated by blue dashed arrows, the maximal rate of oxidative phosphorylation (ATPmax) is measured. P_i decreases back to resting levels and pH is no longer reliable.

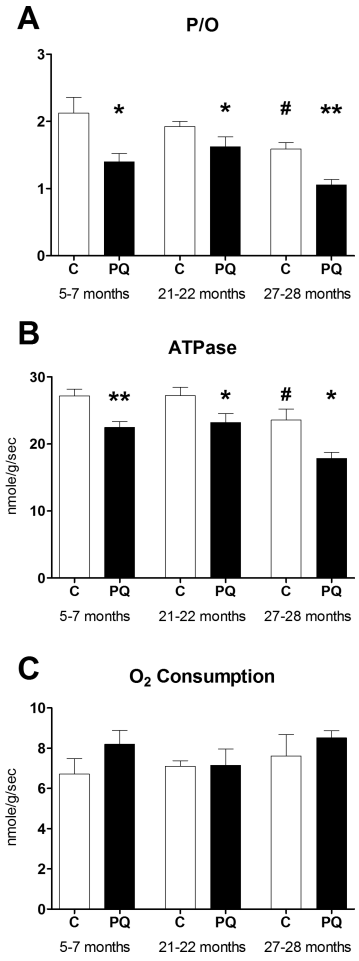

Fig. 4. PQ-treatment leads to reduced P/O throughout life

(A) In vivo P/O ratio decreases 24 hours after PQ-treatment in young, middle aged, and old mice. Reduced P/O is associated with reduced resting ATPase rate (B) without significant changes in mitochondrial O_2 consumption (C) following PQ treatment. The same trend led to a significant decrease in P/O of old relative to young control mice. Data presented as mean ± SEM, n = 4-8, * $p < 0.05$, **$p<0.01$ relative to age-matched control, #$p<0.05$ relative to young control.

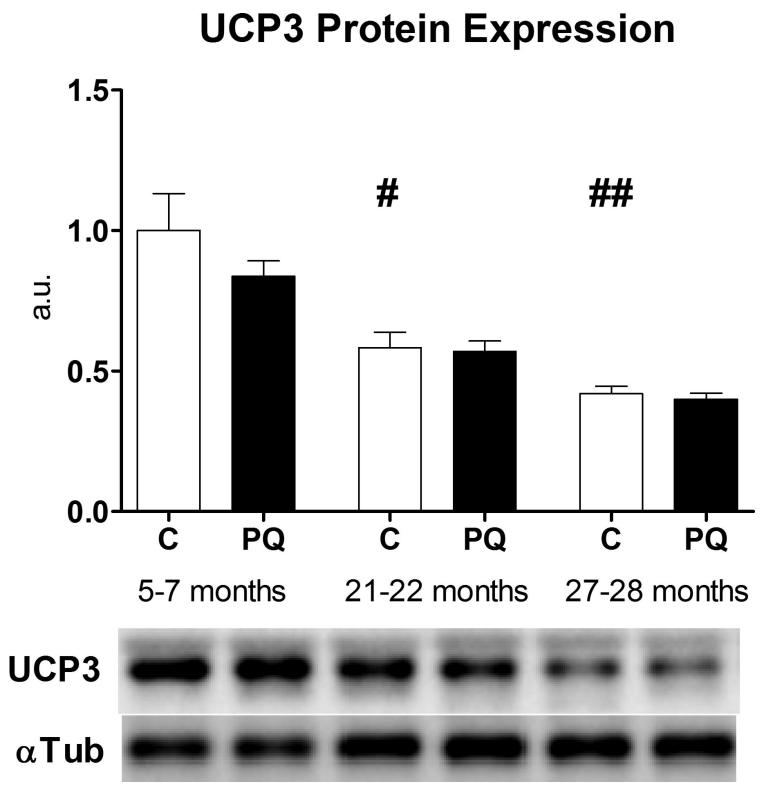

Fig. 5. UCP3 protein expression declines with age

UCP3 protein expression decreases with age, but is unaltered with PQ-treatment, in mixed gastrocnemius. Band densities were normalized to α-tubulin loading control and are presented relative to young control average. Data presented as mean ± SEM, n = 4, #p<0.05, ##p<0.01 relative to young control.

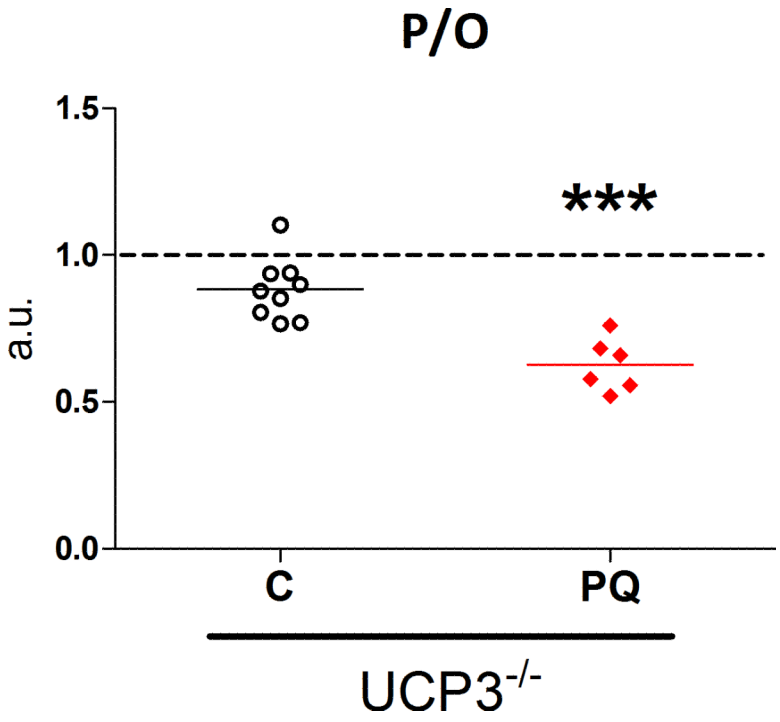

Fig. 6. PQ-treatment leads to reduced P/O in UCP3$^{-/-}$ mice

PQ-treatment leads to reduced coupling of oxidative phosphorylation (decreased P/O) in young adult UCP3$^{-/-}$ mice. Values presented as fraction of P/O ratio in untreated wild type littermate (UCP$^{+/+}$ mice). n = 6-9, *** $p < 0.001$, PQ-treated vs. saline treated (C) UCP3$^{-/-}$ mice. Dashed line represents average P/O for untreated UCP3$^{+/+}$ littermates.

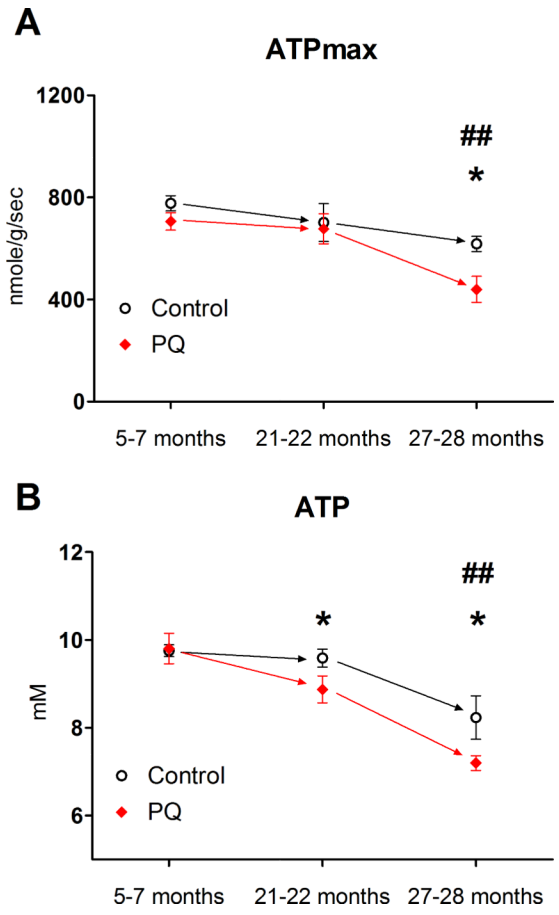

Fig. 7. The energetic consequences of ROS-induced uncoupling are amplified by age

(A) ATPmax was significantly lower in old compared to young controls and PQ treatment led to a significant decline in ATPmax in old mice only. (B) ATP concentration in mixed skeletal muscle decreased significantly in old compared to young controls, and PQ treatment led to significant decreases in ATP in both middle aged and old mice. Data presented as mean ± SEM, n = 4-8, *$p<0.05$ PQ-treatment vs. age-matched control, ## $p<0.01$ aged control vs. young control.

Table 1

In vivo metabolite concentrations in mixed skeletal muscle. ATP and Cr were determined using HPLC from skeletal muscle frozen after in vivo experiments and the remaining values were calculated using the fully relaxed in vivo MR spectra.

	5-7 Months		21-22 Months		27-28 Months		UCP3-/-	
	C	**PQ**	**C**	**PQ**	**C**	**PQ**	**C**	**PQ**
ATP(mM)	9.76±0.14	9.81±0.35	9.59±0.20	8.87±0.31*	8.23±0.50$^{\#\#}$	7.20±0.17*	9.67±0.29	9.28±0.37
PCr(mM)	35.48±1.05	31.97±1.48*	33.86±1.10	27.70±0.95**	29.26±0.76$^{\#\#\#}$	24.93±1.13**	33.61±1.29	30.67±2.09
Total Cr(mM)	42.3±0.45	43.01±1.11	43.45±1.44	40.39±1.54	39.33±1.25$^{\#}$	37.28±0.84	40.69±0.81	40.28±0.62
ADP(μM)	14.4±2.6	26.4±1.1**	23.7±3.8	38.9±4.5*	31.4±4.0$^{\#\#}$	27.1±5.8	17.1±2.9	26.0±6.1
AMP(nM)	21.6±6.7	64.8±6.0**	62.8±20.9	161.7±30.5**	110.5±21.3**	105.7±41.4	34.2±11.2	92.2±41.8
AMP/ATP(×10^{-6})	2.21±0.70	6.67±0.77**	6.59±2.2	18.1±3.3**	13.1±1.9$^{\#\#\#}$	14.9±6.0	3.6±1.2	11.0±5.6
PCr/ATP	3.64±0.11	3.26±0.06*	3.53±0.08	3.13±0.09**	3.57±0.09	3.46±0.13	3.48±0.09	3.29±0.13
pH_{Rest}	7.02±0.01	7.04±0.03	7.09±0.02	7.12±0.02	7.11±0.03$^{\#}$	6.97±0.02**	7.06±0.02	7.08±0.03
$pH_{Ischemia}$	6.94±0.01	6.92±0.02	6.95±0.01	6.92±0.01*	6.97±0.01$^{\#}$	6.93±0.01	6.96±0.03	6.93±0.04

Data presented as mean ± SEM, n = 4-8

* $p < 0.05$

** $p<0.01$ relative to age-matched control.

$^{\#}$ $p < 0.05$

$^{\#\#}$ $p<0.01$

$^{\#\#\#}$ $p<0.001$ relative to young control.